Ultrafast X-ray Absorption Spectroscopy Reveals Excited State Dynamics of B_{12} Coenzymes Controlled by the Axial Base.

Taewon Chung[1,§], Taylor P. McClain[3,§], Roberto Alonso-Mori[4], Matthieu Chollet[4], Aniruddha Deb[1], Angel T. Garcia-Esparza[5], Joel Huang Ze En[1], Ryan M. Lamb[1], Lindsay B. Michocki[1], Marco Reinhard[5], Tim B. van Driel[4], James E. Penner-Hahn[1,3],* and Roseanne J. Sension[1,2]*

[1]Department of Chemistry, University of Michigan, 930 N University Ave. Ann Arbor, Michigan, 481091055, U.S.A.

[2]Department of Physics, University of Michigan, 450 Church Street, Ann Arbor, Michigan, 48109-1040, U.S.A.

[3]Biophysics, University of Michigan, 930 N University Ave. Ann Arbor, Michigan, 48109-1055, U.S.A.

[4]Linac Coherent Light Source, SLAC National Accelerator Laboratory, 2575 Sand Hill Road, Menlo Park, CA 94025, U.S.A.

[5]SLAC National Accelerator Laboratory, Stanford Synchrotron Radiation Light Source 2575 Sand Hill Rd. Menlo Park, CA, US 94025-7015

*Corresponding Author e-mail: rsension@umich.edu, Phone: 734-763-6074; jeph@umich.edu.

§ These two authors contributed equally to this work.

Abstract

Polarized time-resolved X-ray absorption spectroscopy at the Co K-edge is used to probe the excited state dynamics and photolysis of base-off methylcobalamin and the excited state structure of base-off adenosylcobalamin. For both molecules, the final excited state minimum shows evidence for an expansion of the cavity around the Co ion by ca. 0.04 Å to 0.05 Å. The 5-coordinate base-off cob(II)alamin that is formed following photodissociation has a structure similar to that of 5-coordinate base-on cob(II)alamin, with a ring expansion of 0.03 Å to 0.04 Å and a contraction of the lower axial bond length relative to that in the 6-coordinate ground state. These data provide insights into the role of the lower axial ligand in modulating the reactivity of B_{12} coenzymes.

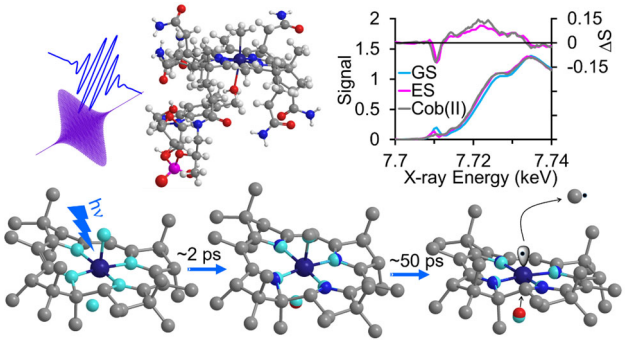

INTRODUCTION

Cobalamins, coenzyme B_{12} and related compounds (see Figure 1), comprise an important class of biological cofactors.[1] In these compounds, low-spin six-coordinate Co(III) is equatorially coordinated to 4 nitrogens from the corrin ring, axially to a lower ligand (called the α ligand in much cobalamin literature), often dimethylbenzamidazole, and an upper ligand (often called the β ligand). The identity of the upper ligand (labeled R in Figure 1) varies, with methylcobalamin (MeCbl) and 5′-deoxyadenosylcobalamin (AdoCbl) being the biologically active coenzymes that are used in essential mammalian enzymes, including two human enzymes, methylmalonyl coA mutase and methionine synthase.[2,3] In the reduced cob(II)alamin form of the cofactor, the upper ligand is missing and the Co is 5-coordinate.

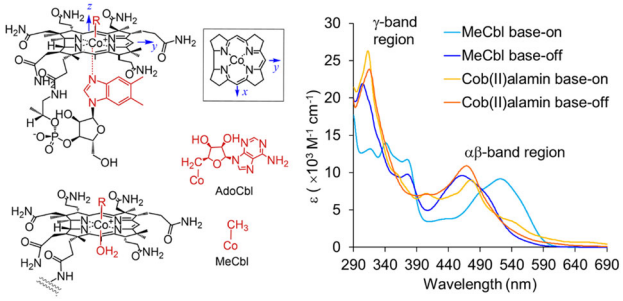

Figure 1. Left: Schematic diagram of base-on and base-off cobalamin. The axis system used in our work is defined in the top row. Right: UV-visible absorption spectrum of base-on MeCbl (pH 7), base-off MeCbl (pH 2), base-on cob(II)alamin (pH 7) and base-off cob(II)alamin (pH 2). The αβ-band region in the visible and the γ-band region in the UV are indicated on the plot. Spectra of the base-on and base-off forms of AdoCbl are plotted in Figure S1.

Cobalamins perform diverse functions in nature such as catalyzing radical rearrangement or facilitating methyl transfer in humans[2] and regulating gene expression in certain bacteria.[4] While the enzymatic activity involves thermal chemistry, gene regulation exploits the photochemistry of cobalamins. Much of the biophysical characterization of cobalamins has focused on the role of the

upper ligand; however, the lower ligand is also important in modulating reactivity. This is evident in the B_{12} trafficking system, which involves elaborate changes in both oxidation state and axial ligation.[5-7] The lower ligand for both AdoCbl and MeCbl is usually a nitrogenous base – either the endogenous dimethylbenzymidazole group or a histidine residue from the protein. However, both can also be prepared in a base-off form with no nitrogenous lower ligand. As one example of the latter, the trafficking protein, human adenosyltransferase (ATR), binds cob(II)alamin with no upper ligand in a rare base-off conformation without a nitrogenous lower ligand before adding the 5'-deoxyadenosyl group and delivering AdoCbl to methylmalonyl-CoA mutase where a histidine residue provides the lower ligand.[6] The oxidation state and ligation play an important role in modulating the reactivity of the cobalamin throughout this process. This conversion from nitrogenous to non-nitrogenous lower ligand can be mimicked chemically by lowering the pH sufficiently (~pH 2) to protonate the dimethylbenzimidazole, resulting the in the spectral changes shown in Figure 1. In parallel with the biochemical nomenclature, we refer to these as base-on MeCbl or AdoCbl at pH ~7 and base-off MeCbl or AdoCbl at pH ~2.

Like ground state reactivity, the photochemical pathways in cobalamins are influenced both by axial ligation and by the environment.[8-17] In particular, photochemical yields are modified by the presence or absence of a nitrogenous lower ligand.[8,18] Replacement of the benzimidazole ligand with water in base-off AdoCbl results in a slightly shorter excited state lifetime, 60 ps compared with 100 ps, and a smaller quantum yield for bond dissociation, 0.12 ± 0.06 compared with ~1.[8] In contrast, replacement of the benzimidazole with water in base-off MeCbl results in a large decrease in the excited state lifetime from 1 ns to 47 ps, but an ~ 4-fold increase in the quantum yield for bond dissociation to 0.65 ± 0.15[8] compared with values ranging from 0.25 (excitation at 400 nm) to <0.15 (excitation in the $\alpha\beta$ band) for base-on MeCbl.[18-20] These observations can be

understood by recognizing that replacement of the benzimidazole ligand with water in the base-off forms of both AdoCbl and MeCbl opens a channel for competition between bond dissociation and internal conversion and recovery of the ground state population that is not available to the base-on compounds.

In the present paper, we use X-ray absorption near-edge structure (XANES) spectroscopy to probe the structure of the excited states of base-off MeCbl and AdoCbl prior to photodissociation and to compare these structures with the base-on compounds. We also compare the structures of the base-on and base-off cob(II)alamin photoproducts. These comparisons highlight important similarities and differences as a function of the axial ligation.

EXPERIMENTAL METHODS

Methylcobalamin and adenosylcobalamin were purchased from MilliporeSigma and used as received. Solutions were prepared by dissolving the cobalamin in deionized water to produce ~0.6 mM solutions for UV-visible measurements and ~5 mM solutions for X-ray absorption measurements. Sample preparation took place under red light to avoid photolysis. Hydrochloric acid (1 M stock solution) was used to lower the pH of the solution to ~2, producing base-off MeCbl or AdoCbl. Solutions for UV-visible measurements were deoxygenated by bubbling with nitrogen for at least an hour and were maintained under a positive pressure of nitrogen during measurements. The sample circulated through a fused silica flow cell with an optical path length of 1 mm to refresh the sample between laser pulses. For XANES measurements, the samples were filtered, then centrifuged, and finally pumped through a glass nozzle to achieve a stable 50 μm diameter jet of solution. Samples were monitored using UV-visible absorption to ensure that any buildup of photoproducts remained insignificant.

UV-Visible Transient Absorption. UV-visible TA spectra of MeCbl were obtained as

reported previously.[8] New measurements of MeCbl at pH 2 were performed to characterize the response in the γ-band region (280 nm to 390 nm) as the earlier measurements only covered the region down to 350 nm.[8] Briefly, a 1 KHz Ti:sapphire laser system produced ca. 70 fs compressed pulses centered around 814 nm. These pulses were frequency doubled in a β-barium borate crystal to ca. 407 nm. A portion of the 407 nm beam was used to pump the base-off MeCbl sample and a second portion was used to produce a broadband continuum probe in a translating CaF_2 window. All measurements were performed with the polarization of the pump and probe pulses at magic angle (54.7°) with respect to each other.

XANES Measurements. XANES difference spectra as a function of visible laser excitation, $\Delta S(t) = S_{on}(t) - S_{off}$, of base-off MeCbl at pH ~2 were obtained for time delays of ca. 0.8 ps, 10 ps and 250 ps using the XCS instrument of the X-ray free electron laser LCLS at SLAC.[21] An additional measurement of base-off AdoCbl at pH ~2 was obtained at ca. 10 ps. The X-ray beam and laser beam travel in a nearly collinear geometry (~1° crossing angle) and were overlapped with the sample about 500 μm from the nozzle producing the sample jet. The optical pump pulse was 490 nm, ~50 fs FWHM and the X-ray probe pulse (~50 fs) was scanned from 7.7 to 7.78 keV. Cobalt X-ray fluorescence was collected with an epix100 detector and used as a measure of X-ray absorption, where the signal was normalized to the small-angle scattering from the solvent measured using a epix10k detector. Both the optical and X-ray pulses were linearly polarized. A waveplate in the optical beam was used to rotate the polarization in order to acquire transient spectra with the polarization of the optical pulse either parallel or perpendicular to the X-ray pulses. The incident beam energy was scanned using a channel-cut Si[111] monochromator with ~3 seconds per energy. Spectra were collected at fixed delay times of 0.8 and 250 ps (base-off MeCbl) and 10 ps (base-off AdoCbl). In addition, data were collected for MeCbl over delays ranging from

5 to 15 ps in a sawtooth pattern with a period of ~1 minute and binned according to delay time. The signal did not vary over this range and was averaged to obtain a ca. 10 ps difference spectrum.

Computational Methods. The Finite Difference Method Near Edge Structure (FDMNES) program was used to simulate the ground and excited state XANES spectra as a function of molecular structure.[22,23] For most FDMNES simulations the cobalamin structure was truncated by removing the tail and replacing the peripheral groups on the corrin ring with methyl groups (Figure S6). Simulations performed with different truncations are compared in Figure S7.

The quantum chemical package Orca 4.2.1[24,25] was used to perform time-dependent density functional theory (TD-DFT) calculations with the B3LYP functional, ZORA-def2-TZVP basis, and CPCM solvent to model the pre-edge region of the ground state spectra of base-on and base-off MeCbl and cob(II)alamin. These calculations were performed on a truncated structure replacing the peripheral groups on the corrin ring with hydrogen. Some calculations were performed without the CPCM solvent model and these spectra are nearly identical to those presented here. Optical transient absorption measurements were fit to a model consisting of a sum of exponential decay components using the global analysis program Glotaran.[26]

RESULTS

UV-Visible Absorption

UV-visible transient absorption (UV-vis TA) spectra of base-off MeCbl were measured from 280 nm to 390 nm. The region from 280 nm to 350 nm is particularly valuable in the characterization of cobalamin dynamics, as it allows one to follow the evolution of γ-band transitions as the molecule moves through electronic states. These data were scaled to the data reported earlier[8] using the overlapping region from 350 nm to 390 nm. The data were then interpolated onto a consistent time grid and the combined UV-vis TA spectra for base-off MeCbl

are summarized in Figure 2. Three excited state species, together with a long-lived cob(II)alamin photoproduct were identified in the earlier study[8] and the transients in the γ-band region are consistent with this analysis. We will designate the three excited state species of base-off MeCbl as **A** ($\tau_A \approx 0.36$ ps), **B** ($\tau_B = 2.1 \pm 0.4$ ps), and **C** ($\tau_C = 47 \pm 4$ ps).[8] A contour plot highlighting the early time behavior and kinetics at select wavelengths illustrating the need for all three decay components are included in Supporting Information Figures S2 and S3.

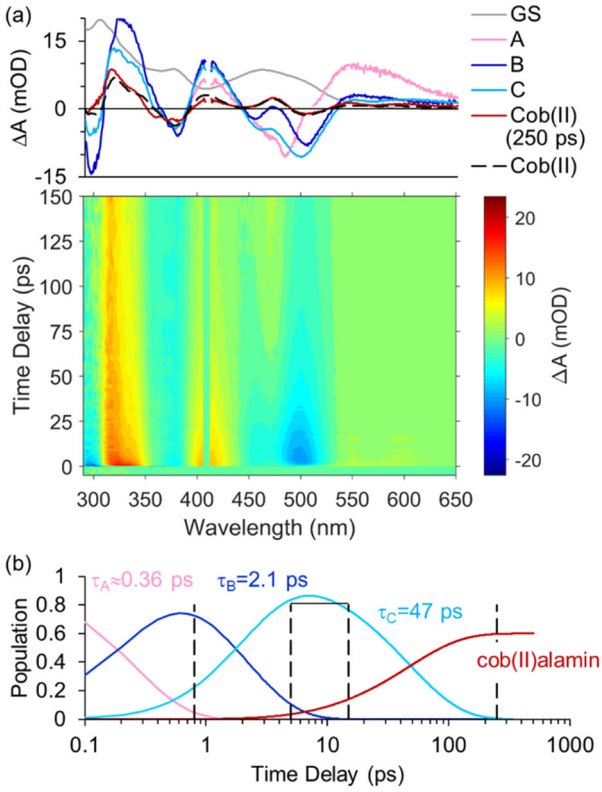

Figure 2. (a) Summary of UV-visible transient absorption measurements for base-off MeCbl following excitation at 407 nm. The data for wavelengths >350 nm was reported previously.[8] The evolution associated difference spectra derived from the data shown in the surface plot are plotted above on the same wavelength scale for direct comparison. The ground state spectrum of base-off MeCbl (gray line) is also plotted for comparison. The spectrum of the short-lived species **A** is complicated by stimulated Raman scattering around 470 nm and by stimulated Raman scattering and cross phase modulation for wavelengths below 380 nm. The region below 380 nm is omitted

from the plot for this species. The Cob(II) difference spectrum at 250 ps (red line) is compared with the difference spectrum that is obtained by subtracting the base-off MeCbl spectrum from that for authentic cob(II)alamin at pH ~2 (black dashed line, see text for details). (b) Time dependent populations of **A**, **B**, **C**, and cob(II)alamin as determined from a global analysis of the transient absorption spectra.[8] The vertical lines represent the time-delays used to measure excited-state XANES for **B** and cob(IIalamin , and the time-delay range used to measure excited-state XANES for **C**.

The long-lived photoproduct can be conclusively identified as cob(II)alamin by comparison with the steady-state photolysis product. Anaerobic photolysis of AdoCbl was used to obtain the spectrum of cob(II)alamin at pH ~2 that is plotted in Figure 1. The reference spectrum was generated using AdoCbl rather than MeCbl because direct photolysis of MeCbl at low pH is complicated by the rapid formation of secondary products. Even under anaerobic conditions, aquocobalamin is the only product observed following steady-state illumination. Fortunately, the steady state absorption spectrum of cob(II)alamin is independent of the initial alkylcobalamin that is used for photolysis. The spectrum plotted in Figure 1 is consistent with those reported earlier for base-off cob(II)alamin,[8,27] and with that observed for base-off cob(II)alamin bound to adenosyltransferase,[6] but is now extended to include the γ-band region. As illustrated in the top panel of Figure 2, the static difference spectrum between MeCbl and cob(II)alamin at pH 2 is consistent with the time-resolved difference spectrum obtained 250 ps after excitation of base-off MeCbl at 407 nm, demonstrating that the long-lived product observed in the transient absorption measurement is base-off cob(II)alamin.

The excited state and product spectra can be estimated from the difference spectra in Figure 2 using:

$$A_{ES} = \Delta A \cdot \alpha + A_{GS} \quad (1)$$

where α is a scale factor depending on the excitation fraction, the quantum yield for excited state or product formation, and the differences in concentration and path length for the steady state absorption measurement of A_{GS} and the transient absorption measurements. The steady state cob(II)alamin spectrum and the reported quantum yield for bond homolysis of 0.65 ± 0.15 were used to constrain α for base-off MeCbl.[8] The estimated excited state spectra for φ=0.65 are plotted in Figure 3. There is some ambiguity to these spectra, since the limiting range of possible φ values runs from ~0.50 to ~0.80. However, excited state spectra for these limiting values (see Figure S4) have qualitatively similar features to those shown in Figure 3.

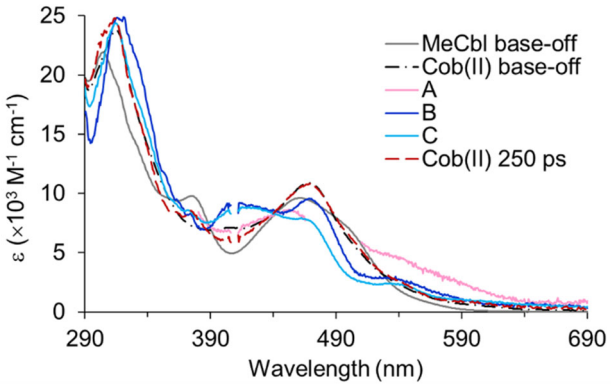

Figure 3. Estimated excited state UV-visible spectra for base-off MeCbl. The spectrum of the short-lived species **A** is complicated by stimulated Raman scattering around 470 nm and by stimulated Raman scattering and cross phase modulation for wavelengths below 380 nm. These regions are omitted from the plot. For reference, the ground-state spectra of the starting base-off MeCbl (gray line) and authentic Cob(II)alamin (dashed-dot black line) are also included. The latter shows that the 250 ps spectrum is identical to Cob(II)alamin.

The excited state spectra of base-off MeCbl are distinctive, differing from the spectra of ground state base-off cob(III)alamins. The initial excited state **A** is characterized by a broad absorption with significant intensity to the red of the ground state absorption. The subsequent excited states are characterized by a broad absorption extending to the red with peaks around 530

nm and 473 nm, a broader absorption peaking around 420 nm and strong γ-band absorption peaks at 316 nm (**B**) and 312 nm (**C**) with shoulders around 338 nm. There is no evidence for a pronounced γ-band absorption in the initial excited state **A** (see Figure S3). The transition from **B** to **C** is characterized primarily by a decrease in the intensity of the peak at 473 nm and a sharpening of the γ-band peak.

Time-Resolved XANES Measurements

Polarized time-resolved XANES measurements were performed for base-off MeCbl following excitation at 490 nm and time delays of ca. 0.8 ps, between 5 ps and 15 ps, and at 250 ps, as indicated by the vertical dashed lines in Figure 2(b). The difference spectrum did not change between 5 and 15 ps and these data were averaged to obtain the ca. 10 ps difference spectrum reported below. Data was obtained using parallel and perpendicular polarization with the isotropic difference signal calculated as $\Delta S = (\Delta S_{\parallel} + 2\Delta S_{\perp})/3$. The isotropic difference spectra are compared with the ground and estimated excited state spectra in Figure 4(a). A difference spectrum for base-off AdoCbl was also obtained for a time delay of 10 ps to allow a comparison of the excited states for these two molecules. The comparison is plotted in Figure 4(b).

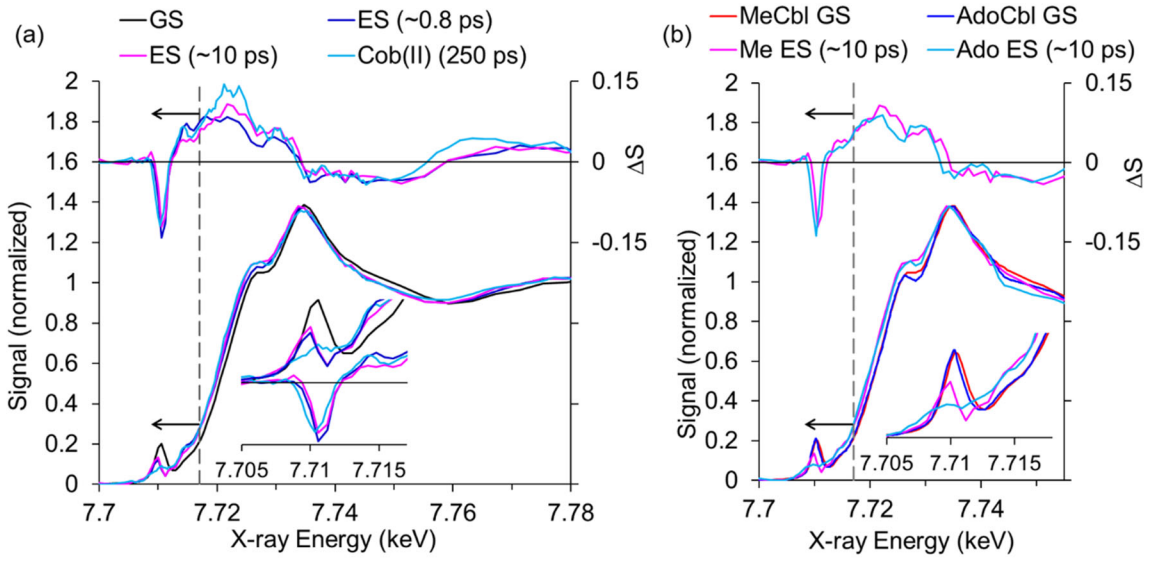

Figure 4. (a) Experimental isotropic difference spectra (ΔS, see text) for base-off MeCbl at different times (top) and the estimated excited state spectra at the same times, calculated using Eq. 2. All XANES spectra are normalized to an edge jump of 1 at 7.78 keV and plotted with the scale on the left axis. The difference spectra are plotted with the amplitude on the right axis. For comparison, the ground state XANES spectrum of base-off MeCbl (black line) and for Cob(II)alamin (light blue line) are included on the lower plot. The vertical dashed line indicates the energy below which the pre-edge transitions dominate. The inset emphasizes the changes in the pre-edge region and shows both the XANES and the difference spectra, scaled vertically in order to highlight the energy shift. (b) Equivalent plot to (a), comparing the ground state XANES spectrum of base-off MeCbl and base-off AdoCbl and their estimated excited state spectra at 10 ps.

The estimated excited state spectra are calculated from the difference spectra using:

$$S_{ES} = \frac{\Delta S_{\parallel} + 2\Delta S_{\perp}}{3} f \cdot \varphi + S_{GS} \qquad (2)$$

where f is the excitation fraction and φ is the yield for excited state or product formation. For both base-off MeCbl and base-off AdoCbl the yield is ~1 at 0.8 ps and ≥0.8 at ca. 10 ps. The yield for the formation of cob(II)alamin from MeCbl is ~0.65 at 250 ps.[8] Under our conditions, the excitation fraction for MeCbl at ca. 0.8 ps and AdoCbl at 10 ps was approximately 0.5 (it must be >0.4 for MeCbl and >0.33 for AdoCbl to retain positive absorption in the pre-edge region). The optical laser power was lower for one pair of scans at 0.8 ps and all scans of MeCbl at ca. 10 ps and 250 ps, giving a lower excitation fraction of approximately 0.4 (it must be >0.3 to retain positive absorption in the pre-edge region). There is no evidence in the data for photoproducts from non-linear absorption.[28] The UV-visible transient absorption of base-off AdoCbl exhibits decay times of 0.5 ps, 2.9 ps, and 60 ps resulting in population evolution similar to that plotted for base-off MeCbl in Figure 2(b),[8] thus the 10 ps difference spectra represent the relaxed excited state (**C**) for both complexes.

The polarization decomposition of the transient XANES spectra provides more insight into the evolution of MeCbl on the excited state surface. The signal obtained with parallel and perpendicular polarization is used to determine the contribution along the transition dipole that is initially excited, designated "*x*", and the sum of the two perpendicular directions, designated "*y*+*z*".

$$\begin{aligned} \Delta S_x &= 2\Delta S_{\parallel} - \Delta S_{\perp} \\ \Delta S_{y+z} &= 3\Delta S_{\perp} - \Delta S_{\parallel} \end{aligned} \tag{3}$$

The transition dipole lies in the corrin ring and thus ΔS_x probes equatorial changes in structure, while ΔS_{y+z} includes both equatorial and axial contributions. The orientation of *x* and *y* in the molecular frame of the corrin is shown in Figure 1. The *z* axis is perpendicular to the plane of the corrin.

The decomposition of the XANES difference spectra for base-off MeCbl is plotted in Figure 5. The most significant changes in the pre-edge and edge region are polarized perpendicular to the transition dipole that was initially excited. The observation that the pre-edge bleach is perpendicular to *x* is consistent with theoretical predictions of the ground-state pre-edge spectra (see below). These predict that the 1*s*-3*d* transition for the ground state of MeCbl should be primarily *z*-polarized as a result of significant mixing of Co 4p_z character with the σ* 3d_{z^2} orbital. Given this, anything that causes a change in the 1*s*-3*d* transition is expected to be primarily z polarized. The edge region, which is mostly sensitive to changes in structure, is also primarily polarized perpendicular to *x*. Given the approximate 4-fold symmetry of the corrin ring, ΔS_x and ΔS_y are likely to be similar, thus Figure 5 provides a qualitative indication (discussed in more quantitative detail below) that most of the structural distortion in the base-off MeCbl excited state is in the z direction.

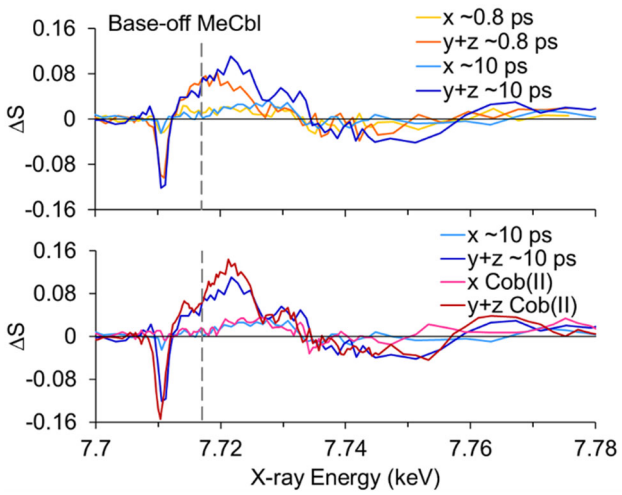

Figure 5. Decomposition of the XANES difference spectra of base-off MeCbl for time delays around 0.8 ps, between 5 and 15 ps, labeled ~10 ps, and at 250 ps, labeled Cob(II), into contributions along (x) and perpendicular (y+z) to the transition dipole initially excited. The vertical dashed line indicates the approximate energy below which pre-edge transitions dominate the spectrum.

The relatively high excitation fractions (see above) could limit the polarization discrimination. However, the observation that there are times and energy ranges in Figure 5 for which the decomposition shows a difference signal in only one of the two possibilities (x or y+z) demonstrates that the polarization discrimination was effective in these data.

DISCUSSION

Within the first picosecond following excitation of base-off MeCbl, the X-ray absorption edge shifts to lower energy. This is reflected in the increase in ΔS_{y+z} at ~7.72 keV. In addition, the x-component of the difference signal exhibits a small increase in intensity in the region from 7.72 to 7.73 keV, characteristic of a small expansion of the corrin ring around the cobalt. However, the most pronounced change at 0.8 ps is in the pre-edge region below 7.717 keV, reflecting changes in the bound orbitals and the electron distribution. Between 0.8 ps to 10 ps there is an additional shift of the edge to lower energy and more substantial changes in the XANES region above 7.717

keV. The intensity of the *x*-polarized contribution increases slightly (see Figures 4 and 5), but there is no significant change in the pre-edge region (Figure 4). The changes in the optical absorption spectrum between 0.8 ps and 10 ps are primarily a blue-shift and narrowing of the excited state γ-band and a decrease in the intensity of an excited state peak at 473 nm (Figure 3). It is likely that the transition from **B** to **C** identified in the optical transient absorption measurements of base-off MeCbl corresponds to structural relaxation on the S_1 excited state surface to a minimum energy structure with a slightly larger ring distortion and with axial bond elongation. Quantum calculations of the pre-edge transitions and FDMNES simulations of the XANES spectra can shed more light on the differences between these states.

Simulations

Ground State MeCbl

The ground state XANES spectra of base-on[29] and base-off MeCbl were simulated using the FDMNES program[22,23] beginning with the crystal structure for ethylcobalamin reported by Hannibal et al.[30] and replacing the ethyl group with a methyl group. While several crystal structures are available for MeCbl,[31-33] the axial bond lengths are shorter (Co-C 1.98-1.99 Å, Co-N_{DMB} 2.16-2.20 Å) than for the other alkylcobalamins (Co-C 2.00-2.03 Å, Co-N_{DMB} 2.23-2.24 Å).[30,32,34] This is not consistent with our measurements of solution-phase XANES spectra for MeCbl, AdoCbl, and n-propylcobalamin, where the spectra are almost indistinguishable (see Figure S5) suggesting that all of the alkylcobalamins have similar structures. It may be that radiation damage contributes to some of these apparent structural differences.[35] To facilitate XANES simulation over a wide range of potential structures, the chosen crystal structure was truncated by replacing the peripheral groups around the corrin ring with methyl groups and by truncating the dimethylbenzimidazole ligand to benzimidazole. This was found to give good agreement with calculations using a more

complete structure, but significantly shortened the calculations and reduced the time and memory required for each calculation (see Figures S6 and S7). A Co-C bond length ca. 2.000 ± 0.025 Å and a Co-N_{DMB} bond length of 2.23 ± 0.01 Å results in a simulated XANES spectrum in good agreement with the measured spectrum (see Figure 6). Base-off MeCbl was simulated by removing the benzimidazole group and replacing it with a water molecule at 2.36 Å as predicted in DFT calculations.[36] The observation that FDMNES-simulated XANES spectra only match the experimental spectra if the Co-C bond lengths and the corrin ring structures are similar for base-on and base-off MeCbl is consistent with prior DFT simulations of a base-on and base-off MeCbl model system.[36] The experimental and simulated XANES spectra of base-off MeCbl are compared with the base-on spectra in Figure 6. In principle, it is possible that base-off MeCbl might contain a 5-coordinate cobalt; for example, no lower α-ligand is identified in the crystal structure of base-off MeCbl bound to CblC.[37] However, removing the lower ligand entirely results in a simulated XANES spectrum that does not agree well with the experimental spectrum (see Figure S8).

TD-DFT calculations of the pre-edge region demonstrate that the change in the lower axial ligand from N to a loosely ligated water molecule at 2.36 Å can account for both the red-shift and the intensity increase in the *z*-polarized $1s \rightarrow 3d_{z^2}$ transition. The slight (≤0.25 eV) decrease in $1s \rightarrow 3d_{z^2}$ energy is consistent with a slightly smaller ligand field for base-off relative to base-on.[38,39] The dipole allowed intensity in this transition is a result of mixing of Co $4p_z$ character into the nominal $3d_{z^2}$ orbital. Again, removing the lower ligand entirely results in a predicted spectrum that is not in good agreement with the experimental data (see Figure S7). Although different results have been reported regarding which functional is best for simulated UV-visible spectra of highly covalent molecules such as cobalamins,[40,41] we find qualitatively similar results for the X-ray absorption with B3LYP and BP86.

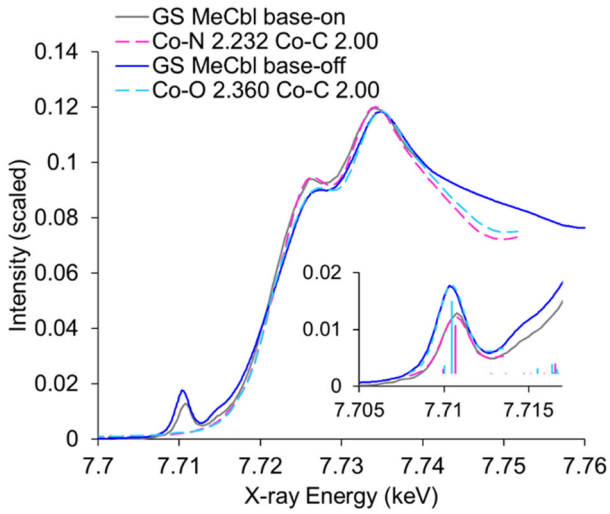

Figure 6. Comparison of the ground state spectrum of base-on MeCbl at pH ~7 and base-off MeCbl at pH 2 with FDMNES simulations. The ring is held constant and the axial bond lengths in Å are given in the legend. TD-DFT simulations of the pre-edge transitions are plotted in the inset. The inclusion of water in the base-off calculation is required for good agreement with experiment (see Figure S7).

Cob(II)alamin

Anaerobic photolysis of alkylcobalamins in the presence of a radical scavenger results in bond homolysis and the formation of a stable cob(II)alamin radical species. The UV-visible absorption spectra of base-on cob(II)alamin produced at neutral pH and base-off, water-on cob(II)alamin observed at low pH are qualitatively similar. Both exhibit a visible absorption band in the blue region of the spectrum peaking at 475 nm (base-on) or 468 nm (base-off) and a γ-band peaking 313 nm or 315 nm for base-on and base-off respectively (see Figures 1 and S9). The similarity in the XANES spectra plotted in Figure S9 suggests that the ligation at the cobalt is similar for both molecules. The base-on cob(II)alamin XANES spectrum is consistent with loss of the upper axial ligand and a decrease in the Co-N_{DMB} bond length to ca. 2.15 Å, accompanied by a small increase in the size of the equatorial cavity for the Co^{2+} radical as illustrated in Figure 7. The contraction

of the Co-N_{DMB} bond to ca. 2.15 Å is in good agreement with the available crystal structures of cob(II)alamin species[42,43] and with quantum chemical calculations.[27,44,45] In contrast, expansion of the Co-N_{corrin} bonds, while not surprising given the larger size of Co(II) relative to Co(III), is not predicted in the quantum chemical calculations or apparent in the crystal structures. However, the increase in XAS intensity around 7.729 keV is only reproduced in FDMNES simulations if a ring expansion is included. In the absence of a ring expansion, the simulated difference signal in this region is uniformly negative as a result of the changes in the axial direction. The large number of potential parameters involved in a distortion and/or expansion of the corrin ring precludes any detailed examination of the structure of the ring at this time. A symmetric expansion resulting in an 0.03 Å increase in the Co-N_{corrin} distance was used for qualitative comparisons with the experimental data.

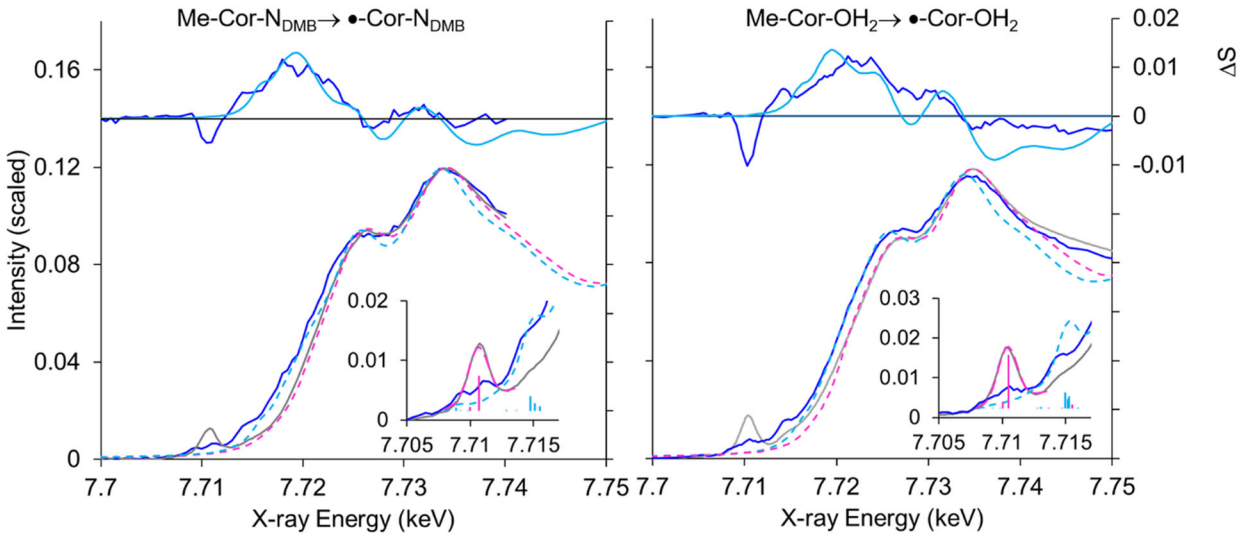

Figure 7. Comparison of the ground state spectrum of base-on (left) and base-off (right) MeCbl (gray) and cob(II)alamin (blue) . FDMNES was used to simulate the XANES spectra and the simulated spectra are plotted as a pink dashed line (MeCbl) and a light-blue dashed line (Cob(II)alamin). Experimental (dark blue) and calculated (light blue) differences for MeCbl minus Cob(II)alamin are plotted at the top of each figure. Both sets of absorption spectra use the vertical

scale shown on the left; both sets of difference spectra use the scale shown on the right. TD-DFT calculations of the pre-edge transitions are plotted in the insets and compared with the experimental spectra.

Base-off cob(II)alamin is also five-coordinate[46] and a contraction of the Co-O bond relative to base-off MeCbl is anticipated based on reported DFT calculations of H_2O-cob(II)inamide. Stich et al. report a Co-O bond length of 2.20 Å,[47] while Li et al. report a Co-O bond length of 2.29 Å.[48] Consistent with this, a contraction of the Co-O distance to 2.20 Å accompanied by a symmetric ring expansion resulting in an 0.04 Å increase in the Co-N_{corrin} distance is in good agreement with the experimental data as plotted in the right hand panel of Figure 7.

Using the structures deduced from the XANES spectra and FDMNES simulations, TD-DFT calculations were performed to model the pre-edge transitions of the cob(II)alamin species. Although a single determinantal model is incomplete for describing open shell systems, we and others[49] have found these to give effective predictions of the relative intensity and energies. The calculations predict red-shifted $3d_{z^2}$ orbitals with $3d_{z^2}(\alpha)$ occupied and $1s\rightarrow 3d_{z^2}(\beta)$ the lowest energy transition, red-shifted ~1.5 to 2 eV from the ground state $1s\rightarrow 3d_{z^2}$ transitions. In addition, *z*-polarized transitions with significant $1s\rightarrow 3d_{z^2}$ character are also observed ca. 5 eV blue-shifted from the ground state transitions for both compounds (Figure 7 insets), in good qualitative agreement with the shoulders observed in the product spectra, although the intensity of this band is over-estimated for base-off cob(II)alamin.

Excited State Structural Dynamics of Base-Off MeCbl.

FDMNES simulations were used to model the structural changes in the excited states **B** (τ_B=2.1 ps) and **C** (τ_C=47 ps) both assigned to the S_1 excited state surface. Reasonable agreement is obtained for **B** using a symmetric expansion of 0.02 Å around the cobalt, although the agreement

for the *y*+*z* contribution improves if the expansion of the Co-O bond is increased to 0.04 Å. This simulation is compared with the 0.8 ps measurement in the left column of Figure 8. Reasonable agreement for **C** requires a larger symmetric expansion of ca. 0.04 Å around the cobalt as illustrated in the center column of Figure 8. Although the parameters used in these simulations do not represent unique fits to the data, it is clear that expansion around the cobalt increases from 0.8 ps to 10 ps following excitation of base-off MeCbl.

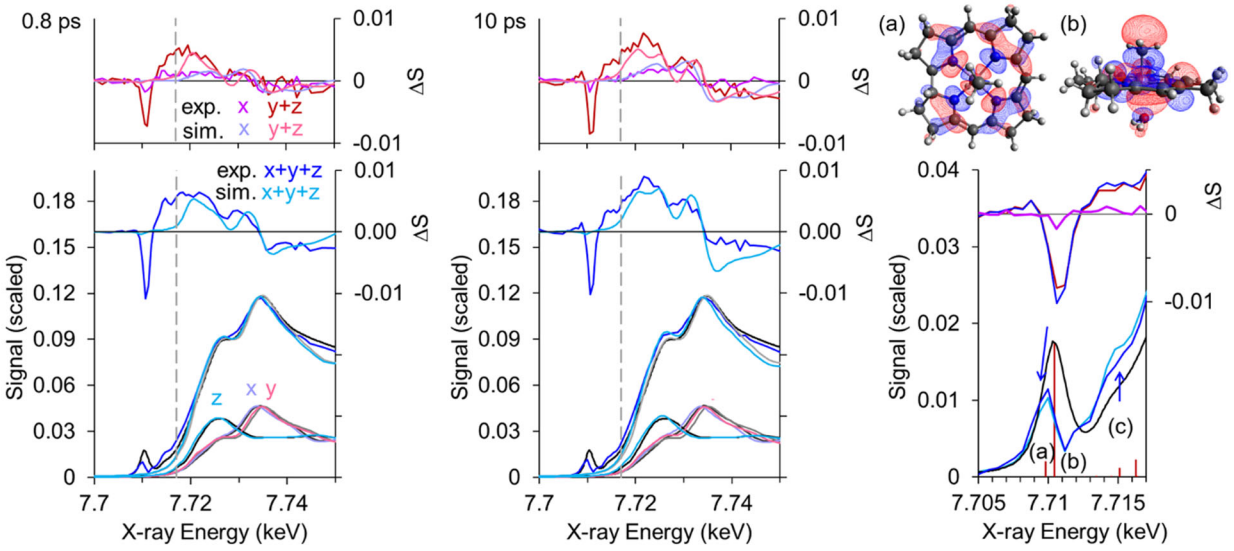

Figure 8. Left: Comparison of the excited state XANES spectrum of the **B** (τ_B=2.1 ps) state of base-off MeCbl with an FDMNES simulation assuming an 0.02 Å symmetric expansion of the corrin ring, an 0.02 Å expansion of the Co-C bond and an 0.04 Å expansion of the Co-O bond. Upper traces shown the experimental and calculated polarized difference spectra (see text) and the experimental and simulated isotropic difference spectra. In the lower plot the black and grey lines represent the experimental and calculated ground state spectra while the colored lines represent the excited state or the difference between the excited state and the ground state. The vertical dashed line indicates the approximate energy below which the pre-edge transitions dominate the spectrum. Center: Similar comparison of the excited state XANES spectrum of the **C** (τ_C=47 ps) state of base-off MeCbl with an FDMNES simulation assuming an 0.04 Å symmetric expansion around the cobalt. The legend is the same as the plot to the left. Right: An enlargement of the pre-edge region

illustrating the difference between the excited and ground states, **B** light blue, **C** dark blue. The TD-DFT simulations of the ground state predict that transitions from the Co 1s orbital to the orbitals plotted above the spectra make the dominant contribution to the indicated transitions. The pre-edge transitions that give rise to the predicted spectra are shown as vertical sticks.

In contrast to the changes apparent in the XANES region (Figure 8) and in the optical absorption spectrum (Figure 3), the pre-edge region of the XAS spectrum is essentially the same for both excited states **B** and **C**. These states are characterized by the bleaching of the $1s \rightarrow 3d_{z^2}$ transition (labeled (b) in Figure 8), an increase in intensity of pre-edge transitions just above 7.715 keV, also with Co $1s \rightarrow d_{z^2}$ character (labeled (c)), and the appearance of a $1s \rightarrow 3d$ transition just below 7.710 keV that is red-shifted from the transition in the ground state. The polarization dependence (see Figure 8) suggests that the dipole-allowed character of this peak is dominated by a transition polarized in the *y* or *z* directions. This is consistent with a shift of the $1s \rightarrow 3d_{z^2}$ transition to lower energy or a depletion of this transition and an increase in the intensity of the $1s \rightarrow d_{xy}$ transition (labeled (a) in Figure 8) in the low energy wing of the ground state pre-edge absorption band. In the TD-DFT calculations, the ground state $1s \rightarrow d_{xy}$ transition (a) derives intensity approximately evenly divided between dipole (*z*-polarized) and quadrupole terms. The change in electron density in the excited state could increase the dipole-allowed contribution to this transition.

Comparison of base-on and base-off excited states

Excitation of base-off MeCbl results in formation of an excited electronic state characterized by expansion of the cavity around the cobalt. The expansion increases as the molecule evolves from **B** at 0.8 ps to **C** at 10 ps. The opposite trend is observed for base-on MeCbl. In this case, excitation in the visible absorption band results in formation of an excited state where rapid

expansion within a picosecond is followed by partial contraction around the cobalt as the molecule relaxes to the excited state minimum (Figure 9(a)). FDMNES simulations of the relaxed excited states for both base-on MeCbl modeled earlier[29] and base-off MeCbl in the present work, suggest an expansion of the cavity around the Co ion by ca. 0.04 to 0.05 Å. The difference spectra are of similar magnitude and shape for both compounds.

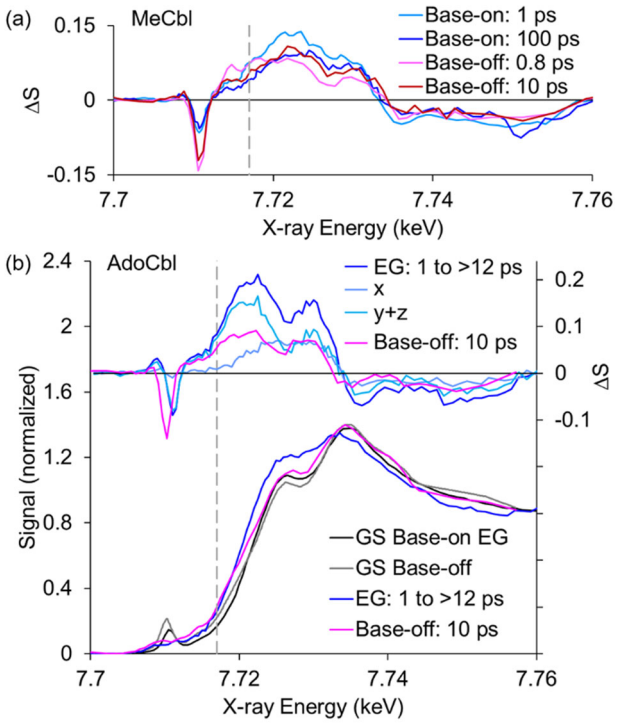

Figure 9. (a) Comparison of the base-on and base-off XANES difference spectra for excitation of MeCbl. The 1 ps spectrum was obtained in the same run as the 100 ps spectrum.[29] The dashed line indicates the approximate break between the pre-edge and XANES regions. (b) Comparison of the ground and estimated excited state XANES spectra for base-on AdoCbl in ethylene glycol (EG)[13,50] and base-off AdoCbl in water.

The differences between base-off and base-on AdoCbl are more significant. An expansion of the cavity around the cobalt is observed in the first picosecond after excitation of base-on AdoCbl with similar differences in water and ethylene glycol solvent.[50] In ethylene glycol, the structure of

the excited state is constant from 1 ps to 12 ps (Figure S4 of ref. [50]) allowing comparison of these spectra with the relaxed excited state of base-off AdoCbl.[11,51,52] In water, an additional excited state structure precedes bond dissociation complicating the interpretation.[51] The base-on and base-off excited state XANES spectra of AdoCbl are compared in Figure 9(b). The structural changes are much larger for base-on AdoCbl than for base-off AdoCbl. This is true for both the ring expansion dominating the x-polarized component and the axial expansion probed by the edge-shift. Work is underway to model these results.

CONCLUSIONS

Polarized X-ray absorption spectroscopy at the Co K-edge provides a powerful tool to unravel excited state dynamics in cobalamins and in transition metal complexes more broadly. In the work reported here, we have used tr-XANES to probe the excited state dynamics and photolysis of base-off MeCbl and to compare the results with changes seen for base-on MeCbl.[29] For both molecules, the final excited state minimum that is populated prior to bond dissociation or ground state recovery shows evidence for an expansion of the cavity around the Co ion by ca. 0.04 Å to 0.05 Å. Despite this structural similarity, the change in cobalt electron distribution in the two molecules appears to be different, as indicated by the red-shifted $1s \rightarrow 3d$ transition that is observed for base-off, but not for base-on MeCbl. The cob(II)alamin that is formed following photodissociation is similar for both base-on and base-off, with a ring expansion of 0.03 Å to 0.04 Å and a contraction of the bond to the lower ligand. The contraction is larger for base-off MeCbl than for base-on MeCbl, however since the starting Co-O distance was longer than the Co-N distance, the end result is a structure with similar bond lengths for both base-on and base-off cob(II)alamin. Interestingly, the excited states of base-on MeCbl, base-off MeCbl, and base-off AdoCbl all recapitulate the structure of the CarH excited state, with only small changes in bond lengths. However, only the

base-on MeCbl gives a long-lived metastable state similar to that seen in CarH, suggesting that changes in axial ligation may similarly be important in controlling the unique behavior that is seen for AdoCbl when bound to CarH.

SUPPORTING INFORMATION

A pdf file including details of data analysis and modeling along with additional figures of experimental data and of FDMNES and orca simulations as a function of structural parameters is available.

DATA AVAILABILITY

The processed data used to produce the figures shown in the manuscript and supporting material are available from DeepBlue (DOI:____). Also available at this site are representative input files to FDMNES and ORCA.

ACKNOWLEDGEMENTS

This work was supported by grants from the National Science Foundation NSF-CHE 1836435, NSF-CHE 2154157 to RJS. Partial support for RAM came from NIH grant P41GM139687. Use of the Linac Coherent Light Source (LCLS), SLAC National Accelerator Laboratory, is supported by the U.S. Department of Energy, Office of Science, Office of Basic Energy Sciences under Contract No. DE-AC02-76SF00515.

REFERENCES

(1) Marques, H. M., The inorganic chemistry of the cobalt corrinoids – an update. *J. Inorg. Biochem.* **2023**, *242*, 112154, 10.1016/j.jinorgbio.2023.112154.

(2) Mascarenhas, R.; Gouda, H.; Ruetz, M.; Banerjee, R., Human B12-dependent enzymes: Methionine synthase and Methylmalonyl-CoA mutase In *Methods in Enzymology*; Marsh, E. N. G., Ed.; Academic Press: 2022; Vol. 668, p 309-326, 10.1016/bs.mie.2021.12.012

(3) Giedyk, M.; Goliszewska, K.; Gryko, D., Vitamin B_{12} catalysed reactions. *Chem. Soc. Rev.* **2015**, *44*, 3391-3404, 10.1039/c5cs00165j.

(4) Padmanabhan, S.; Jost, M.; Drennan, C. L.; Elias-Arnanz, M., A new facet of vitamin B_{12}: Gene regulation by cobalamin-based photoreceptors. *Annu. Rev. Biochem.* **2017**, *86*, 485-514, 10.1146/annurev-biochem-061516-044500.

(5) Banerjee, R.; Gouda, H.; Pillay, S., Redox-Linked Coordination Chemistry Directs Vitamin B-12 Trafficking. *Acc. Chem. Res.* **2021**, *54*, 2003-2013, 10.1021/acs.accounts.1c00083.

(6) Mascarenhas, R.; Ruetz, M.; McDevitt, L.; Koutmos, M.; Banerjee, R., Mobile loop dynamics in adenosyltransferase control binding and reactivity of coenzyme B_{12}. *Proc. Natl. Acad. Sci. U.S.A.* **2020**, *117*, 30412-30422, 10.1073/pnas.2007332117.

(7) McCorvie, T. J.; Ferreira, D.; Yue, W. W.; Froese, D. S., The complex machinery of human cobalamin metabolism. *J. Inherit. Metab. Dis.* **2023**, *46*, 406-420, 10.1002/jimd.12593.

(8) Peng, J.; Tang, K. C.; McLoughlin, K.; Yang, Y.; Forgach, D.; Sension, R. J., Ultrafast Excited-State Dynamics and Photolysis in Base-Off B-12 Coenzymes and Analogues: Absence of the trans-Nitrogenous Ligand Opens a Channel for Rapid Nonradiative Decay. *J. Phys. Chem. B* **2010**, *114*, 12398-12405, 10.1021/jp104641u.

(9) Al Mamun, A.; Toda, M. J.; Lodowski, P.; Kozlowski, P. M., Photolytic Cleavage of Co-C

Bond in Coenzyme B-12-Dependent Glutamate Mutase. *J. Phys. Chem. B* **2019**, *123*, 2585-2598, 10.1021/acs.jpcb.8b07547.

(10) Toda, M. J.; Lodowski, P.; Al Mamun, A.; Jaworska, M.; Kozlowski, P. M., Photolytic properties of the biologically active forms of vitamin B_{12}. *Coord. Chem. Rev.* **2019**, *385*, 20-43, 10.1016/j.ccr.2018.12.017.

(11) Harris, D. A.; Stickrath, A. B.; Carroll, E. C.; Sension, R. J., Influence of environment on the electronic structure of cob(III)alamins: Time-resolved absorption studies of the S_1 state spectrum and dynamics. *J. Am. Chem. Soc.* **2007**, *129*, 7578-7585, 10.1021/ja066197y.

(12) Wiley, T. E.; Miller, N. A.; Miller, W. R.; Sofferman, D. L.; Lodowski, P.; Toda, M. J.; Jaworska, M.; Kozlowski, P. M.; Sension, R. J., Off to the races: Comparison of excited state dynamics in vitamin B_{12} derivatives hydroxocobalamin and aquocobalamin. *J. Phys. Chem. A* **2018**, *122*, 6693-6703, 10.1021/acs.jpca.8b06103.

(13) Miller, N. A.; Kaneshiro, A. K.; Konar, A.; Alonso-Mori, R.; Britz, A.; Deb, A.; Glownia, J. M.; Koralek, J. D.; Mallik, L.; Meadows, J. H.et al.;, The Photoactive Excited State of the B12-Based Photoreceptor CarH. *J. Phys. Chem. B* **2020**, *124*, 10732−10738, 10.1021/acs.jpcb.0c09428.

(14) Sension, R. J.; Harris, D. A.; Stickrath, A.; Cole, A. G.; Fox, C. C.; Marsh, E. N. G., Time-resolved measurements of the photolysis and recombination of adenosylcobalamin bound to glutamate mutase. *J. Phys. Chem. B* **2005**, *109*, 18146-18152, 10.1021/jp052492d.

(15) Sension, R. J.; Cole, A. G.; Harris, A. D.; Fox, C. C.; Woodbury, N. W.; Lin, S.; Marsh, E. N. G., Photolysis and recombination of adenosylcobalamin bound to glutamate mutase. *J. Am. Chem. Soc.* **2004**, *126*, 1598-1599, 10.1021/ja0396910.

(16) Jones, A. R., The photochemistry and photobiology of vitamin B_{12}. *Photochem. Photobiol. Sci.* **2017**, *16*, 820-834, 10.1039/c7pp00054e.

(17) Kutta, R. J.; Hardman, S. J. O.; Johannissen, L. O.; Bellina, B.; Messiha, H. L.; Ortiz-Guerrero, J. M.; Elias-Arnanz, M.; Padmanabhan, S.; Barran, P.; Scrutton, N. S.et al.;, The photochemical mechanism of a B_{12}-dependent photoreceptor protein. *Nat. Commun.* **2015**, *6*, 7907, 10.1038/ncomms8907.

(18) Taylor, R. T.; Smucker, L.; Hanna, M. L.; Gill, J., Aerobic photoiysis of alkylcobalamins: Quantum yields and light-action spectra. *Arch. Biochem. Biophys.* **1973**, *156*, 521-533, 10.1016/0003-9861(73)90301-9.

(19) Shiang, J. J.; Walker II, L. A.; Anderson, N. A.; Cole, A. G.; Sension, R. J., Time-resolved spectroscopic studies of B_{12} coenzymes: The photolysis of methylcobalamin is wavelength dependent. *J. Phys. Chem. B* **1999**, *103*, 10532-10539, 10.1021/jp992358r.

(20) Walker II, L. A.; Jarrett, J. T.; Anderson, N. A.; Pullen, S. H.; Matthews, R. G.; Sension, R. J., Time-resolved spectroscopic studies of B_{12} coenzymes: The identification of a metastable cob(III)alamin photoproduct in the photolysis of methylcobalamin. *J. Am. Chem. Soc.* **1998**, *120*, 3597-3603, 10.1021/ja974024q.

(21) Alonso-Mori, R.; Caronna, C.; Chollet, M.; Curtis, R.; Damiani, D. S.; Defever, J.; Feng, Y.; Flath, D. L.; Glownia, J. M.; Lee, S.et al.;, The X-ray Correlation Spectroscopy instrument at the Linac Coherent Light Source. *J. Synchrot. Radiat.* **2015**, *22*, 508-513, 10.1107/S1600577515004397.

(22) Bunau, O.; Joly, Y., Self-consistent aspects of X-ray absorption calculations. *J. Phys. Condens. Matter* **2009**, *21*, 345501, 10.1088/0953-8984/21/34/345501.

(23) Joly, Y., X-ray absorption near-edge structure calculations beyond the muffin-tin approximation. *Phys. Rev. B* **2001**, *63*, 125120, 10.1103/PhysRevB.63.125120.

(24) Neese, F., Software update: The ORCA program system—Version 5.0. *WIREs Comput. Mol.*

Sci. **2022**, *12*, e1606, 10.1002/wcms.1606.

(25) Neese, F., The ORCA program system. *WIREs Comput. Mol. Sci.* **2012**, *2*, 73-78, 10.1002/wcms.81.

(26) Snellenburg, J. J.; Laptenok, S.; Seger, R.; Mullen, K. M.; van Stokkum, I. H. M., Glotaran: A Java-based graphical user interface for the R package TIMP. *J. Stat. Soft.* **2012**, *49*, 1-22, 10.18637/jss.v049.i03.

(27) Stich, T. A.; Buan, N. R.; Brunold, T. C., Spectroscopic and Computational Studies of Co2+Corrinoids: Spectral and Electronic Properties of the Biologically Relevant Base-On and Base-Off Forms of Co2+Cobalamin. *J. Am. Chem. Soc.* **2004**, *126*, 9735-9749, 10.1021/ja0481631.

(28) Sension, R. J.; Chung, T.; Dewan, P.; McClain, T. P.; Lamb, R. M.; Penner-Hahn, J. E., Time-resolved spectroscopy: Advances in understanding the electronic structure and dynamics of cobalamins In *Methods in Enzymology: Coenzyme B_{12} Enzymes Part B*; Marsh, E. N. G., Ed.; Academic Press: 2022, p 303-331, 10.1016/bs.mie.2022.01.010

(29) Michocki, L. B.; Miller, N. A.; Alonso-Mori, R.; Britz, A.; Deb, A.; Glownia, J. M.; Kaneshiro, A. K.; Konar, A.; Meadows, J. H.; Sofferman, D. L.et al.;, Probing the excited state of methylcobalamin using polarized time-resolved X-ray absorption spectroscopy. *J. Phys. Chem. B* **2019**, *123*, 6042-6048, 10.1021/acs.jpcb.9b05854.

(30) Hannibal, L.; Smith, C. A.; Smith, J. A.; Axhemi, A.; Miller, A.; Wang, S.; Brasch, N. E.; Jacobsen, D. W., High Resolution Crystal Structure of the Methylcobalamin Analogues Ethylcobalamin and Butylcobalamin by X-ray Synchrotron Diffraction. *Inorg. Chem.* **2009**, *48*, 6615-6622, 10.1021/ic900590p.

(31) Randaccio, L.; Furlan, M.; Geremia, S.; Slouf, M.; Srnova, I.; Toffoli, D., Similarities and

differences between cobalamins and cobaloximes. Accurate structural determination of methylcobalamin and of LiCl- and KCl-containing cyanocobalamins by synchrotron radiation. *Inorg. Chem.* **2000**, *39*, 3403-3413, 10.1021/ic0001199.

(32) Mebs, S.; Henn, J.; Dittrich, B.; Paulmann, C.; Luger, P., Electron densities of three B_{12} vitamins. *J. Phys. Chem. A* **2009**, *113*, 8366-8378, 10.1021/jp902433x.

(33) Rossi, M.; Glusker, J. P.; Randaccio, L.; Summers, M. F.; Toscano, P. J.; Marzilli, L. G., The structure of a B12 coenzyme: methylcobalamin studies by x-ray and NMR methods. *J. Am. Chem. Soc.* **1985**, *107*, 1729-1738, 10.1021/ja00292a046.

(34) Ouyang, L.; Rulis, P.; Ching, W. Y.; Nardin, G.; Randaccio, L., Accurate redetermination of the X-ray structure and electronic bonding in adenosylcobalamin. *Inorg. Chem.* **2004**, *43*, 1235-1241, 10.1021/ic0348446.

(35) Champloy, F.; Gruber, K.; Jogl, G.; Kratky, C., XAS spectroscopy reveals X-ray-induced photoreduction of free and protein-bound B_{12} cofactors. *J. Synchrot. Radiat.* **2000**, *7*, 267-273, 10.1107/S0909049500006336.

(36) Lodowski, P.; Jaworska, M.; Garabato, B. D.; Kozlowski, P. M., Mechanism of Co–C Bond Photolysis in Methylcobalamin: Influence of Axial Base. *J. Phys. Chem. A* **2015**, *119*, 3913-3928, 10.1021/jp5120674.

(37) Koutmos, M.; Gherasim, C.; Smith, J. L.; Banerjee, R., Structural Basis of Multifunctionality in a Vitamin B-12-processing Enzyme. *J. Biol. Chem.* **2011**, *286*, 29780-29787, 10.1074/jbc.M111.261370.

(38) Sarangi, R., X-ray absorption near-edge spectroscopy in bioinorganic chemistry: Application to M–O2 systems. *Coord. Chem. Rev.* **2013**, *257*, 459-472, 10.1016/j.ccr.2012.06.024.

(39) Sarangi, R.; Aboelella, N.; Fujisawa, K.; Tolman, W. B.; Hedman, B.; Hodgson, K. O.;

Solomon, E. I., X-ray Absorption Edge Spectroscopy and Computational Studies on LCuO2 Species: Superoxide−CuII versus Peroxide−CuIII Bonding. *J. Am. Chem. Soc.* **2006**, *128*, 8286-8296, 10.1021/ja0615223.

(40) Kuta, J.; Patchkovskii, S.; Zgierski, M. Z.; Kozlowski, P. M., Performance of DFT in modeling electronic and structural properties of cobalamins. *J. Comp. Chem.* **2006**, *27*, 1429-1437, 10.1002/jcc.20454.

(41) Elmendorf, L. D.; Brunold, T. C., Vibronic coupling in vitamin B12: A combined spectroscopic and computational study. *Inorg. Chem.* **2023**, *62*, 12762–12772, 10.1021/acs.inorgchem.3c01305.

(42) Kräutler, B.; Keller, W.; Kratky, C., Coenzyme B_{12} chemistry: The crystal and molecular structure of cob(II)alamin. *J. Am. Chem. Soc.* **1989**, *111*, 8936-8938, 10.1021/ja00206a037.

(43) Jogl, G.; Wang, X.; Mason, S. A.; Kovalevsky, A.; Mustyakimov, M.; Fisher, Z.; Hoffman, C.; Kratky, C.; Langan, P., High-resolution neutron crystallographic studies of the hydration of the coenzyme cob(II)alamin. *Acta Crystallogr. D* **2011**, *67*, 584-591, doi:10.1107/S090744491101496X.

(44) Demissie, T. B.; Repisky, M.; Liu, H.; Ruud, K.; Kozlowski, P. M., Cob(II)alamin: Relativistic DFT analysis of the EPR parameters. *J. Chem. Theory Comput.* **2014**, *10*, 2125-2136, 10.1021/ct400769t.

(45) Garabato, B. D.; Kumar, N.; Lodowski, P.; Jaworska, M.; Kozlowski, P. M., Electronically excited states of cob(II) alamin: insights from CASSCF/XMCQDPT2 and TD-DFT calculations. *Phys. Chem. Chem. Phys.* **2016**, *18*, 4513-4526, 10.1039/c5cp06439b.

(46) Van Doorslaer, S.; Jeschke, G.; Epel, B.; Goldfarb, D.; Eichel, R.-A.; Kräutler, B.; Schweiger, A., Axial Solvent Coordination in “Base-Off” Cob(II)alamin and Related Co(II)-Corrinates

Revealed by 2D-EPR. *J. Am. Chem. Soc.* **2003**, *125*, 5915-5927, 10.1021/ja021218j.

(47) Stich, T. A.; Buan, N. R.; Escalante-Semerena, J. C.; Brunold, T. C., Spectroscopic and computational studies of the ATP : Corrinoid adenosyltransferase (CobA) from Salmonella enterica: Insights into the mechanism of adenosylcobalamin biosynthesis. *J. Am. Chem. Soc.* **2005**, *127*, 8710-8719, 10.1021/ja042142p.

(48) Li, Z.; Shanmuganathan, A.; Ruetz, M.; Yamada, K.; Lesniak, N. A.; Krautler, B.; Brunold, T. C.; Koutmos, M.; Banerjee, R., Coordination chemistry controls the thiol oxidase activity of the B-12-trafficking protein CblC. *J. Biol. Chem.* **2017**, *292*, 9733-9744, 10.1074/jbc.M117.788554.

(49) Scarborough, C. C.; Sproules, S.; Weyhermüller, T.; DeBeer, S.; Wieghardt, K., Electronic and Molecular Structures of the Members of the Electron Transfer Series [Cr(tbpy)3]n (n = 3+, 2+, 1+, 0): An X-ray Absorption Spectroscopic and Density Functional Theoretical Study. *Inorg. Chem.* **2011**, *50*, 12446-12462, 10.1021/ic201123x.

(50) Miller, N. A.; Michocki, L. B.; Konar, A.; Alonso-Mori, R.; Deb, A.; Glownia, J. M.; Sofferman, D. L.; Song, S.; Kozlowski, P. M.; Kubarych, K. J.et al.;, Ultrafast XANES monitors sequential structural evolution in photoexcited coenzyme B_{12}. *J. Phys. Chem. B* **2020**, *124*, 199-209, 10.1021/acs.jpcb.9b09286.

(51) Yoder, L. M.; Cole, A. G.; Walker II, L. A.; Sension, R. J., Time-resolved spectroscopic studies of B_{12} coenzymes: Influence of solvent on the photolysis of adenosylcobalamin. *J. Phys. Chem. B* **2001**, *105*, 12180-12188, 10.1021/jp012157z.

(52) Sension, R. J.; Harris, D. A.; Cole, A. G., Time-resolved spectroscopic studies of B_{12} coenzymes: A comparison of the influence of solvent on the primary photolysis mechanism and geminate recombination of methyl-, ethyl-, n-propyl-, and 5'-deoxyadenosylcobalamin. *J. Phys. Chem. B* **2005**, *109*, 21954-21962, 10.1021/jp053202w.